Quantitative Structure−Activity Relationship Studies on Inhibition of HERG Potassium Channels

Katsumi Yoshida and Tomoko Niwa*

Discovery Research Laboratories, Nippon Shinyaku Co., Ltd. 14, Nishinosho-Monguchi-cho, Kisshoin, Minami-ku, Kyoto 601-8550, Japan

Received October 12, 2005

The human ether-a-go-go-related gene (HERG) protein forms the ion channel responsible for the rapidly acting delayed rectifier potassium current, I_{Kr}, and its blockade is a significant contributor to prolongation of the QT interval. Using descriptors which have clear physicochemical meanings and are familiar to medicinal chemists, we have carried out 2D-quantitative structure−activity relationship (2D-QSAR) studies on 104 HERG channel blockers with diverse structures collected from the literature, and we have formulated interpretable models to guide chemical-modification studies and virtual screening. Statistically significant descriptors were selected by a genetic algorithm, and the final model included the octanol/water partition coefficient, topological polar surface area, diameter, summed surface area of atoms with partial charges from −0.25 to −0.20, and an indicator variable representing the experimental conditions. The statistics were $r = 0.839$, $r^2 = 0.704$, $q^2 = 0.671$, $s = 0.763$, and $F = 46.6$. The correspondence of the molecular determinants derived from the 2D-QSAR models with the 3D structural characteristics of the putative binding site in a homology-modeled HERG channel is also discussed.

INTRODUCTION

The human ether-a-go-go-related gene (HERG) encodes the rapidly acting delayed rectifier potassium current (I_{Kr}) channel. Inhibition of I_{Kr} by drugs and their metabolites causes prolongation of the QT interval, an effect which can lead to cardiac arrhythmias and sudden death, and several marketed drugs have been withdrawn because of their cardiovascular toxicity. The experimental determination of the blocking effects of drugs is time-consuming and expensive. An attractive alternative solution is in silico screening, that is, predicting the blocking effects of drugs by computational methods. By such methods, large numbers of compounds can be handled easily and rapidly. Another great advantage of in silico screening is its ability to predict the blocking effects of new compounds not yet synthesized.

There are many computational methods for predicting biological activities, such as traditional two-dimensional quantitative structure−activity relationships (2D-QSAR), three-dimensional quantitative structure−activity relationships (3D-QSAR), and docking studies based on the 3D structures of target receptors. Ekins et al.[1] have constructed a 3D-QSAR pharmacophore model with Catalyst; Cavalli et al.[2] have reported a comparative molecular field analysis study of HERG channel blockers, and Pearlstein et al.[3] have carried out comparative molecular similarity indices 3D-QSAR and homology modeling studies. It is generally assumed in 3D-QSAR studies that drugs bind to HERG channels in a similar way. However, there may be some variation in the mode of binding, because the inner pore of HERG is very large, and there is great structural variation among HERG channel blockers. Our preliminary 3D-QSAR studies suggested that the use of multiple 3D-QSAR models gives better results than a single 3D-QSAR model (unpublished data).

Recently, Keseru[4] has developed traditional and hologram QSAR models to predict HERG potassium channel affinities. The advantage of 2D- and hologram QSAR models is that one need not make explicit assumptions about the modes of binding or the binding sites. For the analysis of the complicated affinities of HERG-channel blockers, 2D-QSAR seems to be more robust than 3D-QSAR. Keseru's models predict well the blocking effects of drugs, but the descriptors used are not particularly familiar to medicinal chemists. It is very important for medicinal chemists to understand the characteristic structural factors that could cause QT interval prolongation. To be practically useful, predictive models should be easily interpretable. The objective of the present study was to derive readily interpretable 2D-QSAR models by using descriptors which are familiar to medicinal chemists and which have clear physicochemical meanings. We have derived 2D-QSAR models based on 104 HERG channel blockers with diverse structures collected from the literature, and we have elucidated the molecular determinants responsible for QT interval prolongation. The correspondence of the molecular determinants derived from 2D-QSAR models with the 3D structural characteristics of the putative binding site in a homology-modeled HERG channel is also discussed.

METHODS

IC_{50} values for drugs with HERG-channel-blocking activity were gathered from the literature. We carefully noted the experimental conditions described in every reference, and we selected the IC_{50} data obtained from measurements of

* Corresponding author tel.: +81-75-321-9010; fax: +81-75-321-9038; e-mail: t.niwa@po.nippon-shinyaku.co.jp.

10.1021/ci050450g CCC: $33.50
Published on Web 03/23/2006

Table 1. Experimentally Measured pIC_{50} Values of 104 Drugs Used in This Study

drug	pIC_{50}(M)	Cell	ref.	drug	pIC_{50}(M)	Cell	ref.
2-hydroxy methyl olanzapine	4.936	HEK	1	BMCL131829-06	6.863	CHO	3
9-hydroxy risperidone	5.886	HEK	1	BMCL131829-07	6.883	CHO	3
alfuzosin	4.079	CHO	5	BMCL131829-08	7.444	CHO	3
alosetron	5.495	HEK	1	BRL-32872	7.703	HEK	10
ambasilide	5.444	CHO	6	canrenoic acid	3.982	CHO	11
amitriptyline	5.000	CHO	7	chlorpromazine	5.833	CHO	7
astemizole	9.046	HEK	8	ciprofloxacin	3.015	CHO	12
azimilide	6.252	CHO	6	cisapride	7.347	CHO	3
bepridil	7.585	HEK	9	citalopram	5.401	CHO	13
BMCL131829-01	7.056	CHO	3	clarithromycin	4.483	HEK	14
BMCL131829-10	8.208	CHO	3	clozapine	6.495	HEK	1
BMCL131829-11	6.337	CHO	3	clozapine n-oxide	3.875	HEK	1
BMCL131829-13	7.629	CHO	3	CO-101244	6.161	CHO	15
BMCL131829-14	6.690	CHO	3	cocaine	5.143	HEK	16
BMCL131829-15	7.959	CHO	3	DC-loratidine	5.740	HEK	5
BMCL131829-16	4.585	CHO	3	desipramine	5.857	HEK	1
BMCL131829-17	5.830	CHO	3	desmethyl erythromycin	3.832	HEK	14
BMCL131829-18	5.342	CHO	3	desmethyl olanzapine	4.848	HEK	1
BMCL131829-19	5.711	CHO	3	desmethylastemizole	9.000	HEK	8
BMCL131829-02	8.000	CHO	3	diltiazem	4.762	HEK	17
BMCL131829-20	4.804	CHO	3	disopyramide	5.141	CHO	18
BMCL131829-21	5.658	CHO	3	dofetilide	8.000	CHO	3
BMCL131829-22	5.456	CHO	3	dolasetron	5.225	HEK	19
BMCL131829-03	8.155	CHO	3	domperidone	6.790	CHO	20
BMCL131829-04	6.237	CHO	3	doxazosin	6.233	HEK	22
BMCL131829-05	5.125	CHO	3	droperidol	7.492	HEK	24
E-4031	7.742	HEK	1	nicotine	3.611	HEK	1
ER-118585	7.390	HEK	25	norastemizole	7.558	HEK	8
erythromycin	4.141	HEK	14	olanzapine	6.636	HEK	1
erythromycylamine	3.562	HEK	14	oleandomycin	3.469	HEK	14
fexofenadine	4.638	CHO	3	ondansetron	6.093	HEK	19
flecainide	5.408	HEK	23	perhexiline	5.108	CHO	31
fluoxetine	5.824	CHO	13	pimozide	7.745	CHO	3
gatifloxacin	3.886	CHO	12	prazosin	5.804	HEK	22
granisetron	5.428	HEK	19	propafenone	6.357	HEK	23
grepafloxacin	4.301	CHO	12	quetiapine	5.239	CHO	32
halofantrine	7.666	HEK	21	quinidine	6.387	HEK	23
haloperidol	7.495	CHO	3	risperidone	6.830	HEK	1
imipramine	5.469	CHO	26	roxithromycin	4.438	HEK	14
irbesartan	3.714	CHO	27	sertindole	8.523	CHO	3
josamycin	3.990	HEK	14	sildenafil	5.481	HEK	1
ketoconazole	5.721	HEK	1	sparfloxacin	4.745	CHO	12
levofloxacin	3.039	CHO	12	spironolactone	4.638	CHO	11
lignocaine	3.580	HEK	23	tamsulosin	3.980	CHO	5
loratadine	6.762	HEK	28	terazosin	4.752	HEK	22
MDL-74156	4.917	HEK	19	terfenadine	7.252	CHO	3
mefloquine	5.251	CHO	29	thioridazine	7.479	HEK	1
mesoridazine	6.495	HEK	1	verapamil	7.027	HEK	9
mizolastine	6.456	HEK	30	vesnarinone	5.975	HEK	33
moxifloxacin	3.889	CHO	12	WO0075109−1	5.398	CHO	15
N-desbutylhalofantrine	7.144	HEK	21	WO0075109−2	5.328	CHO	15
N-desmethylclozapine	5.348	HEK	1	ziprasidone	6.903	HEK	1

HERG channels expressed in HEK (human embryonic kidney) and CHO (Chinese hamster ovary) cells. We tried to exclude references that contain very little experimental data, so as to minimize differences in the experimental conditions. A final list of 104 compounds was compiled (Table 1).

Table 2 lists the descriptors used in modeling. The descriptors were calculated for the neutral forms of the compounds only, because of the difficulty of correctly predicting all possible ionic forms. ClogP and CMR values were calculated with ClogP version 4.41 by BioByte Corporation.[34] The calculation of other descriptors and multiple linear regression analysis were performed with MOE 2004.03 by Chemical Computing Group Inc.[35] A program (ga.svl) written in the scientific vector language and implemented in MOE automated the selection of the relevant descriptors by a genetic algorithm. The default setting was used for descriptor selection except for the initial length (the number of descriptors), which was set to 4 for eq 1 and 5 for eqs 2 and 3. 3D models of HERG channels were built as described by Fernandez et al.[36] on the basis of the crystal structure of the *Methanobacterium thermoautotrophicum* MthK channel in the open state.[37] The docking study was performed with GLIDE version 3.0.[38] The default setting was used in grid generation and docking with the extra precision option, and the best pose was minimized by using the MMFF94 force field[39] implemented in MOE. The ligand and the amino acids within 7 Å of the ligand were fully minimized until the root-mean-square gradient of the potential energy was less than 0.05 kcal mol^{-1} $Å^{-1}$. The graphics were produced with PyMOL version 0.97 (DeLano Scientific, South San Francisco, CA).

Table 2. Descriptors Used in the Analysis

descriptor	definition
Hydrophobicity	
ClogP	octanol/water partition coefficient
CMR	molar refractivity
Charge	
PEOE_VSA	sum of the van der Waals surface area of atoms where the PEOE atomic partial charges are in a predefined range
PEOE_PC	total positive or negative partial charges
Hydrogen Bond	
TPSA	topological polar surface area
atom counts	number of hydrogen-bond donor or acceptor atoms
Shape	
diameter	largest value in the distance matrix

RESULTS

Selection of Descriptors. Nowadays, it is not difficult to calculate many descriptors, so it is not unusual to include a large number of descriptors in modeling.[40] However, we decided to limit the number of descriptors, because the objective of this study was to generate QSAR equations with clear physicochemical meanings. It seems that 3D descriptors based on 3D structures of molecules are better than 2D descriptors based on 2D chemical structures in predicting various properties of drugs. However, there are some disadvantages of using 3D descriptors. First, 3D descriptors demand lengthy and expensive computations, and the calculation of 3D descriptors for a large set of compounds, for example, a combinatorial library, is impracticable. Second, to calculate 3D descriptors, one has to generate the 3D structures of molecules. Because different computational programs result in somewhat different 3D structures, there will be some uncertainties in the calculated 3D descriptors. And third, medicinal chemists are more familiar with 2D descriptors than 3D descriptors. For these reasons, 3D descriptors were not used in this study. Instead, descriptors based on 2D chemical structures were selected (Table 2).

ClogP, CMR, and TPSA are widely used to predict not only biological activity but also absorption, distribution, metabolism, and excretion properties. Hydrogen-bonding interactions are a very important part of receptor−ligand interactions, so the numbers of hydrogen-bond donors and acceptors were calculated. To represent the electronic properties, we selected PEOE_PC and PEOE_VSA descriptors, which are based on the partial charges calculated by the Gasteiger−Marsili method,[41] where PEOE stands for partial equalization of orbital electronegativities. (PEOE_PC represents the total positive or negative partial charges of a molecule, and PEOE_VSA is the sum of the van der Waals surface area of atoms where the atomic partial charges are in a predefined range.) Originally, 14 PEOE_VSA descriptors were defined by using uniform interval boundaries in (−infinity, −0.3, −0.25, −0.20, −0.15, −0.10, −0.05, 0, +0.05, +0.10, +0.15, +0.20, +0.25, +0.30, and +infinity).[35] For example, PEOE_VSA-4 is the sum of the van der Waals surface areas of atoms where the atomic partial charges are in the range of −0.25 to −0.20. Atoms with very small partial charges exert very weak electronic effects, so PEOE_VSA-0 and PEOE_VSA+0, corresponding to the ranges from −0.05 to 0 and from 0 to 0.05, respectively, were not used. PEOE_VSA gives more-detailed information on the electronic properties of molecules than does PEOE_PC, while retaining a clear physicochemical meaning. The diameter defined by Petitjean is a graph-based descriptor and corresponds to the distance from a vertex to the most remote vertex in the graph, where distance is expressed by the number of edges between the two vertexes.[42] (For example, the diameter values for benzene, ethyl benzene, and octan-1-ol are 3, 5, and 8, respectively.) This descriptor was selected to represent the shapes of the drugs.

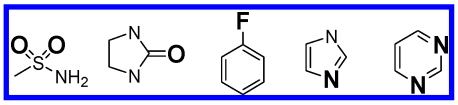

Figure 1. Examples of atoms having nonzero PEOE_VSA-4 values. The atoms shown in bold bear atomic partial charges in the range of −0.25 to −0.20 and have nonzero PEOE_VSA-4 values.

2D-QSAR Models. There are great structural variations in the 104 drugs selected. To include as much structural variation as possible, we used all 104 drugs in the modeling. Relevant descriptors were selected by a genetic algorithm from the 22 descriptors listed in Table 2. We then tested for correlations among the selected descriptors. When an equation contained two descriptors whose correlation coefficient was greater than 0.60, that equation was discarded in order to avoid collinearity problems. Among the remaining equations, the best-performing one was eq 1:

$$\begin{aligned} \mathrm{pIC_{50}} = {} & 0.231(\pm 0.108)\mathrm{ClogP} - 0.014(\pm 0.005)\mathrm{TPSA} + \\ & 0.221(\pm 0.061)\mathrm{diameter} + \\ & 0.029(\pm 0.017)\mathrm{PEOE\_VSA\text{-}4} + 2.592(\pm 0.772) \\ & n = 104,\ r = 0.797,\ r^2 = 0.636,\ q^2 = 0.604, \\ & s = 0.847,\ \text{and}\ F = 43.2 \quad (1) \end{aligned}$$

In QSAR equations, n is the number of data points, r is the correlation coefficient, r^2 is the goodness of fit, q^2 is the leave-one-out cross-validated correlation coefficient expressing the goodness of prediction, s is the standard deviation, and F is the ratio of the variance of the calculated values to that of the observed values. The figures in parentheses are the 95% confidence intervals. Despite the large structural variations, a total of only four of the 22 descriptors was sufficient to explain the blocking effects of the drugs on the HERG potassium channels. As ClogP increases, the blocking effect increases. PEOE_VSA-4 is the sum of the surface areas of atoms with partial charges from −0.25 to −0.20, and representative atoms corresponding to PEOE_VSA-4 are shown in Figure 1. The presence of such atoms increases the blocking activity of the compound. The diameter is the largest value in the distance matrix, and it represents the length of a molecule. As the length increases, the inhibitory effect increases. TPSA is the topological polar surface area, and it represents structural features that donate or accept hydrogen bonds. As TPSA increases, the blocking effect decreases.

Owing to the limited amount of experimental data, $\mathrm{IC_{50}}$ values measured with HERG channels expressed in HEK and CHO cells were analyzed together. To take into account differences in the experimental conditions, we introduced

an indicator variable, "Cell", which is zero for drugs tested with HERG channels expressed in HEK cells and unity for those tested with HERG channels expressed in CHO cells. An improved equation, eq 2, was derived, which justified the combined use of IC_{50} data measured with HERG channels expressed in HEK and CHO cells.

$$\begin{aligned} pIC_{50} = {} & 0.221(\pm 0.097)\text{ClogP} - 0.017(\pm 0.005)\text{TPSA} + \\ & 0.231(\pm 0.055)\text{diameter} + \\ & 0.037(\pm 0.016)\text{PEOE\_VSA-4} - \\ & 0.793(\pm 0.330)\text{Cell} + 2.993(\pm 0.719) \\ & n = 104,\ r = 0.839,\ r^2 = 0.704,\ q^2 = 0.671, \\ & s = 0.763, \text{ and } F = 46.6 \quad (2) \end{aligned}$$

The coefficient of the Cell term is helpful when comparing experimental data measured under different conditions.

Except for ClogP, all of the descriptors in eqs 1 and 2 were calculated with MOE. It would be very convenient if all of the descriptors could be made computable with MOE. To achieve this, we replaced ClogP with SlogP, an atom-based hydrophobic descriptor developed by Wildman and Crippen,[43] to obtain eq 3:

$$\begin{aligned} pIC_{50} = {} & 0.262(\pm 0.143)\text{SlogP} - 0.018(\pm 0.006)\text{TPSA} + \\ & 0.222(\pm 0.060)\text{diameter} + \\ & 0.038(\pm 0.016)\text{PEOE\_VSA-4} - \\ & 0.884(\pm 0.342)\text{Cell} + 2.972(\pm 0.779) \\ & n = 104,\ r = 0.828,\ r^2 = 0.685,\ q^2 = 0.653, \\ & s = 0.787, \text{ and } F = 42.7 \quad (3) \end{aligned}$$

The quality of eq 3 is comparable to that of eq 2. SlogP was shown to perform as well as ClogP, and the correlation between ClogP and SlogP was 0.810. Equation 3 is particularly useful for calculating a large number of pIC_{50} values.

Validation Test. All 104 drugs were used for modeling in order to include as much structural information as possible. It is worthwhile to validate this procedure by modeling with different data sets. The 104 drugs were therefore divided into two sets, a training set of 86 drugs for modeling and a test set of 18 drugs for prediction. The test set was randomly selected. When the 86 drugs in the training set were used, relevant descriptors were selected as for eq 2, and the pIC_{50} values of the remaining 18 drugs were then predicted. This procedure was carried out five times. For all of the runs, the best equation was formulated with ClogP, TPSA, diameter, PEOE_VSA-4, and Cell. This fact clearly shows that these five descriptors are indeed significant ones.

As shown in Table 3, deviations in the coefficients of each descriptor were small among sets 1−5, and the averaged coefficients were very close to the corresponding coefficients in eq 2. The statistics are shown in Table 4. For the training sets, the statistics were comparable to those of eq 2. The statistics of the test sets were not quite as good as those of the training sets, presumably because the number of compounds in the test set was much smaller than that in the training set. Figure 2 shows the correlation between the observed and predicted values for set 1 in Table 3, and Figure 3 shows the chemical structures included in the test set.

Table 3. Coefficients of Equations Formulated with Five Different Training Sets

set[a]	ClogP[b]	TPSA[b]	diameter[b]	PEOE_VSA-4[b]	Cell[b]	constant[b]
1	0.221	−0.018	0.229	0.037	−0.668	3.003
2	0.231	−0.017	0.213	0.043	−0.856	3.207
3	0.211	−0.017	0.254	0.034	−0.815	2.697
4	0.208	−0.018	0.237	0.039	−0.942	3.067
5	0.219	−0.017	0.231	0.039	−0.797	2.950
avg	0.218	−0.017	0.233	0.038	−0.816	2.985

[a] Each set includes 86 drugs for training and 18 drugs for testing, and the average (avg) of the values for the five runs is shown. [b] The coefficient of each descriptor is shown.

Table 4. Statistical Parameters of Equations Formulated with Five Different Training and Test Sets

	training			test		
set[a]	r	r^2	s	r	r^2	s
1	0.839	0.704	0.767	0.829	0.688	0.805
2	0.851	0.723	0.722	0.772	0.596	0.997
3	0.844	0.713	0.761	0.793	0.628	0.849
4	0.838	0.703	0.769	0.836	0.698	0.793
5	0.840	0.705	0.767	0.832	0.693	0.792
avg	0.842	0.710	0.757	0.812	0.661	0.847

[a] Each set includes 86 drugs for training and 18 drugs for testing, and the average (avg) of the values for the five runs is shown.

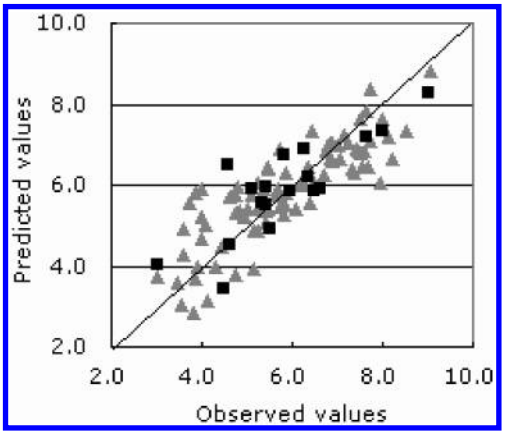

Figure 2. Plot of predicted versus observed pIC_{50} (M) values. The values shown are those obtained with set 1 in Table 3 using eq 2. Triangles and squares represent the compounds in the training and test sets, respectively.

We next examined the predictive abilities of our models by using the data set reported by Keseru,[4] the details of which are provided in the Supporting Information. Because the experimental conditions for Keseru's data set are unavailable, the pIC_{50} values were predicted with eq 1, and the following equation was derived for all 68 drugs analyzed by Keseru:

$$\begin{aligned} pIC_{50} = {} & \\ & 0.912(\pm 0.165)pIC_{50}(\text{predicted}) + 0.325(\pm 1.002) \\ & n = 68,\ r = 0.806,\ r^2 = 0.649,\ s = 0.837, \text{ and} \\ & F = 122.0 \quad (4) \end{aligned}$$

where pIC_{50}(predicted) is the predicted value according to eq 1. Although the selection criteria were different, eq 1 predicted well the pIC_{50} values for Keseru's data set. Of the 68 drugs analyzed by Keseru, 17 were absent from our data set. For these 17 drugs, the correlation between predicted

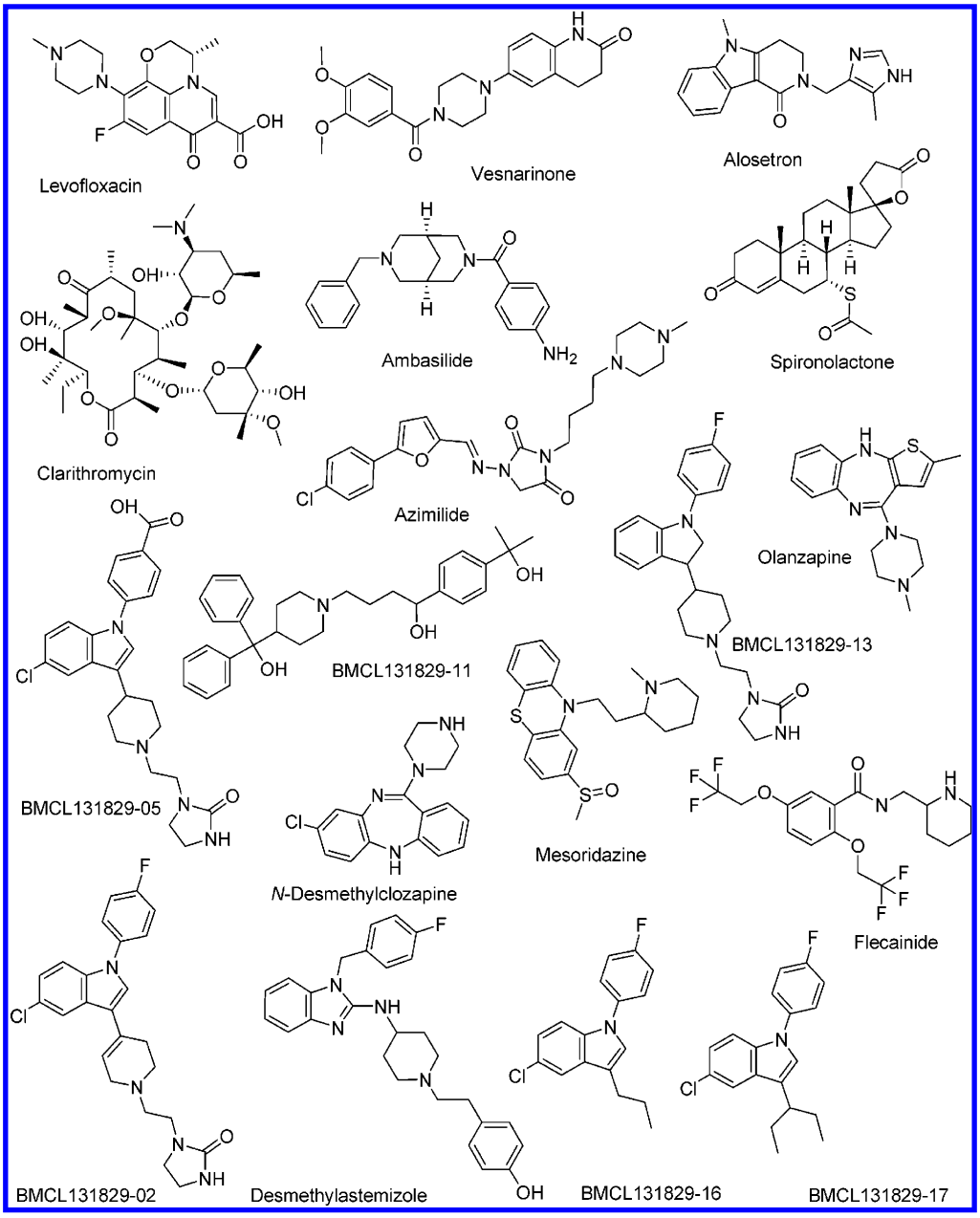

Figure 3. Chemical structures of the compounds included in the test set.

and observed values was examined:

$$pIC_{50} = 0.817(\pm 0.361)pIC_{50}(\text{predicted}) + 0.554(\pm 2.188)$$
$$n = 17,\ r = 0.780,\ r^2 = 0.608,\ s = 1.016,\ \text{and}\ F = 23.2 \quad (5)$$

The statistical quality of the analysis of the 17 drugs was slightly poorer than that of the analyses represented by eqs 1 and 4. Nevertheless, the correlation between the observed and predicted pIC_{50} values was good, and our equations derived with the 104 drugs have good predictive abilities.

DISCUSSION

Structural Characteristics of the HERG Channel. Biologically important proteins such as enzymes generally have unsymmetrical and structurally complicated binding sites in order to strictly distinguish the proper substrates or ligands, which are mostly unsymmetrical. In contrast, the binding site (inner pore) of the HERG channel is symmetric and relatively simple, because four HERG subunits assemble as a tetramer to form the HERG channel.[44] Such a symmetric structure of the inner pore is favorable for the recognition and filtering of symmetric ions but unfavorable for the strict distinguishing of unsymmetrical organic molecules. As a result, HERG channels can accommodate a wide range of molecular structures. Presumably, it is these structural characteristics of HERG channels which have enabled us to build our simple 2D-QSAR models despite the structural diversity in our data set. Fairly simple predictive models have also been published for the blood−brain barrier[45] and membrane permeability,[46] where the partitioning processes involved are not as specific as the binding of drugs to their targets generally is.

Correspondence between 2D-QSAR Models and 3D Structures of HERG Channels. To investigate the structural

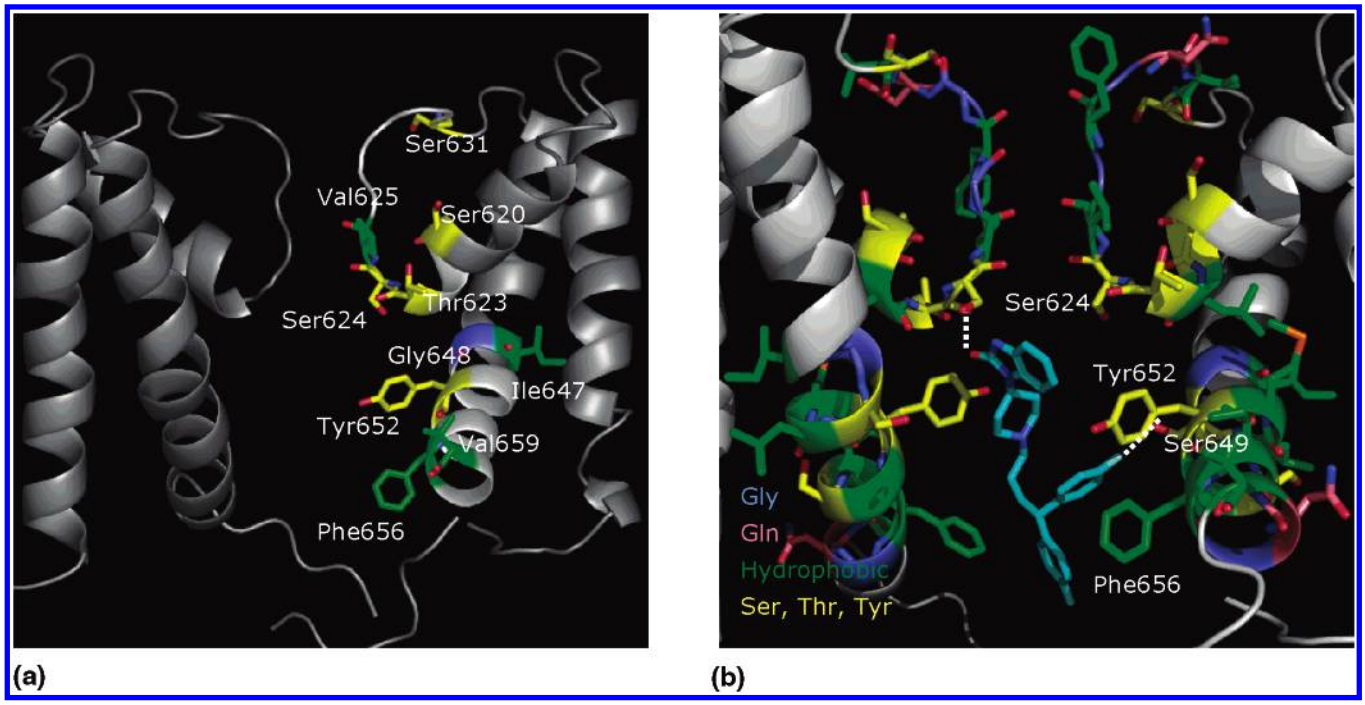

Figure 4. Modeled structure of a HERG channel. (a) Amino acids reported to participate in the binding of drugs[47] are labeled. For simplicity, only two of the four subunits which form the channel are shown. (b) Inner pore region. Amino acids are colored according to their physicochemical properties. Pimozide is shown in blue, and the hydrogen-bonding interactions are shown as white broken lines.

factors responsible for the blockade of HERG channels in more detail, we examined the correspondence of the molecular determinants derived from our 2D-QSAR models with the 3D structural characteristics of the pore region in a homology-modeled HERG channel. The 3D structure was built on the basis of the crystal structure of the *M. thermoautotrophicum* MthK channel in the open state.[37] Figure 4a shows representative amino acids reported to participate in the binding of drugs,[47] and Figure 4b depicts the amino acids in the inner pore region, where pimozide was docked as a representative blocker. (Pimozide was selected because it is highly active and contains atoms having nonzero PEOE_VSA-4 values.) For simplicity, only two of the four subunits of the channel are shown.

The inner pore is very large (Figure 4). In our models, the coefficient with "diameter" (the largest value in the distance matrix) was positive, showing that longer drugs block the channel better. Drugs with large diameter values appear to fill the large inner pore well by adapting their conformations to the space available. The Kv and KCNQ channel families generally have a Pro−Val−Pro or Pro−Ile−Pro motif at positions 655−657 in the S6 domain, whereas the corresponding amino acids in the HERG channel are Ile−Phe−Gly.[47] A lack of structurally rigid prolines in the S6 domain would also favor the binding of longer drugs.

There are four polar amino acids in the inner pore, Thr623, Ser624, Ser649, and Tyr652 (shown in yellow in Figure 4). It is well-known that Tyr652 is an important amino acid for the binding of drugs, and π-cation interactions between Tyr652 and the cationic groups of *N*-protonated drugs have been proposed.[44] According to mutation experiments,[36,48] Thr623 and Ser624 at the base of the pore helix are also involved in drug binding. Ser649 also faces into the inner pore. Because these four residues all have OH groups, they are capable of hydrogen-bonding interactions. The atoms shown in bold in Figure 1, which correspond to the PEOE_VSA-4 values, are capable of forming hydrogen bonds with the OH groups. Other than Thr623, Ser624, Ser649, and Tyr652, the amino acids lining the pore do not have side chains capable of hydrogen-bonding interactions. Therefore, these amino acids are the candidate amino acids which could interact with atoms having nonzero PEOE_VSA-4 values. The hydrogen-bonding interactions of the carbonyl oxygen and fluorine atoms of pimozide with the OH groups are shown as white broken lines in Figure 4b.

In the pore region, half of the amino acids are hydrophobic (shown in green in Figure 4b), and there are no ionizable amino acids, so the pore region is hydrophobic in nature. It is, therefore, to be expected that, in our models, the hydrophobicity of drugs, expressed by the ClogP term, would tend to increase their blocking effect and that their hydrophilicity, represented by TPSA, would tend to decrease their blocking effect. We have previously defined the π_b hydrophobic descriptors for amino acids;[49,50] these descriptors are based on the 1-octanol/water partition coefficients of oligopeptides measured by Akamatsu et al.[51,52] According to our hydrophobic descriptors (Table 5), the most hydrophobic amino acid among those shown in Figure 4 is the Phe at position 656.

Fernandez et al.[36] performed a systematic replacement of Phe656 with 12 alternative amino acids and found a correlation between the IC_{50} values for three drugs (MK-499, cisapride, and terfenadine) and the physicochemical properties of the amino acid at position 656 (see Table 5). The statistically significant descriptors were the hydrophobicity (expressed as the sum of the approximate van der Waals surface areas of atoms deemed hydrophobic in character; VHSA) and the number of nitrogen atoms. Although the π_b values were originally defined for peptides,

Table 5. IC_{50} (μM) Values of MK-499, Cisapride, and Terfenadine Determined for Phe656 Mutant HERG Channels and the Hydrophobic Descriptor π_b for Each Amino Acid

amino acid[a]	MK-499[b]	cisapride[b]	terfenadine[b]	π_b[c]
Phe	0.046	0.124	0.148	1.72
Trp	0.081	0.144	0.215	1.97
Tyr	0.150	0.092	0.094	1.06
Met	0.172	0.103	0.117	0.94
Leu	0.361	0.490	0.131	1.47
Ile	0.493	0.176	0.317	1.37
Val	3.01	1.02	0.668	0.95
Ala	22.20	10.00	3.27	0.16
Gly	61.06	19.77	4.80	0.00
Thr	9.59	17.97	2.75	0.01
Ser	36.85	14.30	3.76	−0.27
Glu	41.74	33.40	3.03	−0.05
Arg	73.82	39.79	9.04	−0.50

[a] Amino acid at position 656. [b] From ref 36. [c] From ref 49.

they have also been shown to be applicable to proteins.[49] The IC_{50} values listed in Table 5 were then analyzed with the π_b values, and the following equations were obtained:

$$pIC_{50}(\text{MK-499}) = 1.374(\pm 0.336)\pi_b - 1.309(\pm 0.351)$$
$$n = 13,\ r = 0.938,\ r^2 = 0.880,\ s = 0.436,\ \text{and}\ F = 80.9 \quad (6)$$

$$pIC_{50}(\text{cisapride}) = 1.201(\pm 0.351)\pi_b - 1.047(\pm 0.366)$$
$$n = 13,\ r = 0.915,\ r^2 = 0.838,\ s = 0.454,\ \text{and}\ F = 56.9 \quad (7)$$

$$pIC_{50}(\text{terfenadine}) = 0.798(\pm 0.253)\pi_b - 0.437(\pm 0.264)$$
$$n = 13,\ r = 0.902,\ r^2 = 0.814,\ s = 0.328,\ \text{and}\ F = 48.2 \quad (8)$$

Other descriptors, such as the number of nitrogen atoms, were statistically insignificant in eqs 6−8, and the π_b values better represented the hydrophobicity of the amino acids than did the VHSA values. Equations 6−8 clearly demonstrate the importance of the hydrophobicity of the amino acid at position 656 for the binding of drugs. In Figure 4b, two fluorobenzenes of pimozide are in close contact with Phe656. While hydrophobic amino acids other than Phe656 do contribute to the hydrophobic environment within the pore region, the hydrophobic interaction between Phe656 and drugs is expected to be particularly important.

CONCLUSION

In this study, we have derived practically useful QSAR models describing the blockade of HERG channels, and they are applicable to both virtual screening and chemical-modification studies. In addition, the structural characteristics responsible for the blockade of HERG channels were interpreted with the aid of modeled 3D structures of HERG channels. The accumulation of knowledge on the mechanism of the blockade of HERG channels is expected to provide powerful help in drug discovery and development.

ACKNOWLEDGMENT

We thank Dr. Gerald E. Smyth for his careful reading of the manuscript and for his useful comments during its preparation.

Supporting Information Available: Tables of predicted values for eqs 1−3 and for eq 4. This material is available free of charge via the Internet at http://pubs.acs.org.

REFERENCES AND NOTES

(1) Ekins, S.; Crumb, W. J.; Sarazan, R. D.; Wikel, J. H.; Wrighton, S. A. Three-dimensional quantitative structure−activity relationship for inhibition of human ether-a-go-go-related gene potassium channel. *J. Pharmacol. Exp. Ther.* **2002**, *301*, 427−434.
(2) Cavalli, A.; Poluzzi, E.; De Ponti, F.; Recanatini, M. Toward a pharmacophore for drugs inducing the long QT syndrome: insights from a CoMFA study of HERG K^+ channel blockers. *J. Med. Chem.* **2002**, *45*, 3844−3853.
(3) Pearlstein, R. A.; Vaz, R. J.; Kang, J.; Chen, X. L.; Preobrazhenskaya, M.; Shchekotikhin, A. E.; Korolev, A. M.; Lysenkova, L. N.; Miroshnikova, O. V.; Hendrix, J.; Rampe, D. Characterization of HERG potassium channel inhibition using CoMSiA 3D QSAR and homology modeling approaches. *Bioorg. Med. Chem. Lett.* **2003**, *13*, 1829−1835.
(4) Keseru, G. M. Prediction of hERG potassium channel affinity by traditional and hologram qSAR methods. *Bioorg. Med. Chem. Lett.* **2003**, *13*, 2773−2775.
(5) Fenichel, R. R. Receptor Binding. http://www.fenichel.net/pages/Professional/subpages/QT/Tables/pbydrug.htm (accessed Mar 2006).
(6) Walker, B. D.; Singleton, C. B.; Tie, H.; Bursill, J. A.; Wyse, K. R.; Valenzuela, S. M.; Breit, S. N.; Campbell, T. J. Comparative effects of azimilide and ambasilide on the human ether-a-go-go-related gene (HERG) potassium channel. *Cardiovasc. Res.* **2000**, *48* (1), 44−58.
(7) Tie, H.; Walker, B. D.; Valenzuela, S. M.; Breit, S. N.; Campbell, T. J. The heart of psychotropic drug therapy. *Lancet* **2000**, *355* (9217), 1825.
(8) Zhou, Z.; Vorperian, V. R.; Gong, Q.; Zhang, S.; January, C. T. Block of HERG potassium channels by the antihistamine astemizole and its metabolites desmethylastemizole and norastemizole. *J. Cardiovasc. Electrophysiol.* **1999**, *10* (6), 836−43.
(9) Fossa, A. A.; Wisialowski, T.; Wolfgang, E.; Wang, E.; Avery, M.; Raunig, D. L.; Fermini, B. Differential effect of HERG blocking agents on cardiac electrical alternans in the guinea pig. *Eur. J. Pharmacol.* **2004**, *486* (2), 209−21.
(10) Thomas, D.; Wendt-Nordahl, G.; Rockl, K.; Ficker, E.; Brown, A. M.; Kiehn, J. High-affinity blockade of human ether-a-go-go-related gene human cardiac potassium channels by the novel antiarrhythmic drug BRL-32872. *J. Pharmacol. Exp. Ther.* **2001**, *297* (2), 753−61.
(11) Caballero, R.; Moreno, I.; Gonzalez, T.; Arias, C.; Valenzuela, C.; Delpon, E.; Tamargo, J. Spironolactone and its main metabolite, canrenoic acid, block human ether-a-go-go-related gene channels. *Circulation* **2003**, *107* (6), 889−95.
(12) Kang, J.; Wang, L.; Chen, X. L.; Triggle, D. J.; Rampe, D. Interactions of a series of fluoroquinolone antibacterial drugs with the human cardiac K+ channel HERG. *Mol. Pharmacol.* **2001**, *59* (1), 122−6.
(13) Witchel, H. J.; Pabbathi, V. K.; Hofmann, G.; Paul, A. A.; Hancox, J. C. Inhibitory actions of the selective serotonin re-uptake inhibitor citalopram on HERG and ventricular L-type calcium currents. *FEBS Lett.* **2002**, *512* (1−3), 59−66.
(14) Volberg, W. A.; Koci, B. J.; Su, W.; Lin, J.; Zhou, J. Blockade of human cardiac potassium channel human ether-a-go-go-related gene (HERG) by macrolide antibiotics. *J. Pharmacol. Exp. Ther.* **2002**, *302* (1), 320−7.
(15) Alanine, A.; Burner, S.; Buettelmann, B.; Heitz Neidhart, M.-P.; Jaeschke, G.; Pinard, E.; Wyler, R. Ethanesulfonyl-piperidine derivatives. WIPO/PCT Patent WO 2000075109.
(16) Zhang, S.; Rajamani, S.; Chen, Y.; Gong, Q.; Rong, Y.; Zhou, Z.; Ruoho, A.; January, C. T. Cocaine blocks HERG, but not KvLQT1+minK, potassium channels. *Mol. Pharmacol.* **2001**, *59* (5), 1069−76.
(17) Zhang, S.; Zhou, Z.; Gong, Q.; Makielski, J. C.; January, C. T. Mechanism of block and identification of the verapamil binding domain to HERG potassium channels. *Circ. Res.* **1999**, *84* (9), 989−98.
(18) Paul, A. A.; Witchel, H. J.; Hancox, J. C. Inhibition of HERG potassium channel current by the class 1a antiarrhythmic agent disopyramide. *Biochem. Biophys. Res. Commun.* **2001**, *280* (5), 1243−50.
(19) Kuryshev, Y. A.; Brown, A. M.; Wang, L.; Benedict, C. R.; Rampe, D. Interactions of the 5-hydroxytryptamine 3 antagonist class of antiemetic drugs with human cardiac ion channels. *J. Pharmacol. Exp. Ther.* **2000**, *295* (2), 614−20.
(20) Drolet, B.; Rousseau, G.; Daleau, P.; Cardinal, R.; Turgeon, J. Domperidone should not be considered a no-risk alternative to cisapride in the treatment of gastrointestinal motility disorders. *Circulation* **2000**, *102* (16), 1883−5.

(21) Mbai, M.; Rajamani, S.; January, C. T. The anti-malarial drug halofantrine and its metabolite N-desbutylhalofantrine block HERG potassium channels. *Cardiovasc. Res.* **2002**, *55* (4), 799−805.
(22) Thomas, D.; Wimmer, A. B.; Wu, K.; Hammerling, B. C.; Ficker, E. K.; Kuryshev, Y. A.; Kiehn, J.; Katus, H. A.; Schoels, W.; Karle, C. A. Inhibition of human ether-a-go-go-related gene potassium channels by alpha 1-adrenoceptor antagonists prazosin, doxazosin, and terazosin. *Naunyn. Schmiedebergs Arch. Pharmacol.* **2004**, *369* (5), 462−72.
(23) Paul, A. A.; Witchel, H. J.; Hancox, J. C. Inhibition of the current of heterologously expressed HERG potassium channels by flecainide and comparison with quinidine, propafenone and lignocaine. *Br. J. Pharmacol.* **2002**, *136* (5), 717−29.
(24) Drolet, B.; Zhang, S.; Deschenes, D.; Rail, J.; Nadeau, S.; Zhou, Z.; January, C. T.; Turgeon, J. Droperidol lengthens cardiac repolarization due to block of the rapid component of the delayed rectifier potassium current. *J. Cardiovasc. Electrophysiol.* **1999**, *10* (12), 1597−604.
(25) Mizuno, H.; Adachi, H.; Kimura, J.; Sawa, Y.; Kakiki, M.; Lansdell, K.; Saito, M.; Kerns, W. D. Cardiovascular assessment of ER-118585, a selective phosphodiesterase 5 inhibitor. *Biol. Pharm. Bull.* **2003**, *26* (12), 1661−7.
(26) Teschemacher, A. G.; Seward, E. P.; Hancox, J. C.; Witchel, H. J. Inhibition of the current of heterologously expressed HERG potassium channels by imipramine and amitriptyline. *Br. J. Pharmacol.* **1999**, *128* (2), 479−85.
(27) Moreno, I.; Caballero, R.; Gonzalez, T.; Arias, C.; Valenzuela, C.; Iriepa, I.; Galvez, E.; Tamargo, J.; Delpon, E. Effects of irbesartan on cloned potassium channels involved in human cardiac repolarization. *J. Pharmacol. Exp. Ther.* **2003**, *304* (2), 862−73.
(28) Crumb, W. J., Jr. Loratadine blockade of K^+ channels in human heart: comparison with terfenadine under physiological conditions. *J. Pharmacol. Exp. Ther.* **2000**, *292* (1), 261−4.
(29) Kang, J.; Chen, X. L.; Wang, L.; Rampe, D. Interactions of the antimalarial drug mefloquine with the human cardiac potassium channels KvLQT1/minK and HERG. *J. Pharmacol. Exp. Ther.* **2001**, *299* (1), 290−6.
(30) Taglialatela, M.; Pannaccione, A.; Castaldo, P.; Giorgio, G.; Annunziato, L. Inhibition of HERG1 K^+ channels by the novel second-generation antihistamine mizolastine. *Br. J. Pharmacol.* **2000**, *131* (6), 1081−8.
(31) Walker, B. D.; Valenzuela, S. M.; Singleton, C. B.; Tie, H.; Bursill, J. A.; Wyse, K. R.; Qiu, M. R.; Breit, S. N.; Campbell, T. J. Inhibition of HERG channels stably expressed in a mammalian cell line by the antianginal agent perhexiline maleate. *Br. J. Pharmacol.* **1999**, *127* (1), 243−51.
(32) Kongsamut, S.; Kang, J.; Chen, X. L.; Roehr, J.; Rampe, D. A comparison of the receptor binding and HERG channel affinities for a series of antipsychotic drugs. *Eur. J. Pharmacol.* **2002**, *450* (1), 37−41.
(33) Katayama, Y.; Fujita, A.; Ohe, T.; Findlay, I.; Kurachi, Y. Inhibitory effects of vesnarinone on cloned cardiac delayed rectifier K^+ channels expressed in a mammalian cell line. *J. Pharmacol. Exp. Ther.* **2000**, *294* (1), 339−46.
(34) *ClogP*, ver. 4.41; BioByte Corp.: Claremont, CA.
(35) *MOE 2004.03*; Chemical Computing Group Inc.: Montreal, Quebec, Canada.
(36) Fernandez, D.; Ghanta, A.; Kauffman, G. W.; Sanguinetti, M. C. Physicochemical Features of the HERG Channel Drug Binding Site. *J. Biol. Chem.* **2004**, *279*, 10120−10127.
(37) Jiang, Y.; Lee, A.; Chen, J.; Cadene, M.; Chait, B. T.; MacKinnon, R. The open pore conformation of potassium channels. *Nature* **2002**, *417*, 523−526.
(38) *GLIDE*, version 3.0; Schrödinger Inc.: Portland, OR.
(39) Halgren, T. A. Merck Molecular Force Field, I: extension of MMFF94 using experimental data, additional computational data, and empirical rules. *J. Comput. Chem.* **1996**, *17*, 490−512.
(40) Wegner, J. K.; Zell, A. Prediction of aqueous solubility and partition coefficient optimized by a genetic algorithm based descriptor selection method. *J. Chem. Inf. Comput. Sci.* **2003**, *43*, 1077−1084.
(41) Gasteiger, J.; Marsili, M. Iterative Partial Equalization of Orbital Electronegativity−A Rapid Access to Atomic Charges. *Tetrahedron* **1980**, *36*, 3219−3228.
(42) Petitjean, M. Applications of the Radius−Diameter Diagram to the Classification of Topological and Geometrical Shapes of Chemical Compounds. *J. Chem. Inf. Comput. Sci.* **1992**, *32*, 331−337.
(43) Wildman, S. A.; Crippen, G. M. Prediction of Physicochemical Parameters by Atomic Contributions. *J. Chem. Inf. Comput. Sci.* **1999**, *39*, 868−873.
(44) Mitcheson, J. S.; Chen, J.; Lin, M.; Culberson, C.; Sanguinetti, M. C. A structural basis for drug-induced long QT syndrome. *Proc. Natl. Acad. Sci. U.S.A.* **2000**, *97*, 12329−12333.
(45) Clark, D. E. Rapid calculation of polar molecular surface area and its application to the prediction of transport phenomena. 2. Prediction of blood−brain barrier penetration. *J. Pharm. Sci.* **1999**, *88*, 815−821.
(46) Niwa, T. Using general regression and probabilistic neural networks to predict human intestinal absorption with topological descriptors derived from two-dimensional chemical structures. *J. Chem. Inf. Comput. Sci.* **2003**, *43*, 113−119.
(47) Recanatini, M.; Poluzzi, E.; Masetti, M.; Cavalli, A.; De Ponti, F. QT Prolongation Through Herg K^+ Channel Blockade: Current Knowledge and Strategies for the Early Prediction During Drug Development. *Med. Res. Rev.* **2005**, *25*, 133−166.
(48) Kamiya, K.; Mitcheson, J. S.; Yasui, K.; Kodama, I.; Sanguinetti, M. C. Open channel block of HERG K^+ channels by vesnarinone. *Mol. Pharmacol.* **2001**, *60*, 244−253.
(49) Sotomatsu-Niwa, T.; Ogino, A. Evaluation of the Hydrophobic Parameters of the Amino Acid Side Chains of Peptides and their Application in QSAR and Conformational Studies. *THEOCHEM* **1997**, *392*, 43−54.
(50) Niwa, S. T.; Ogino, A. Multiple Regression Analysis of the Beta-Sheet Propensity of Amino Acids. *THEOCHEM* **1997**, *419*, 155−160.
(51) Akamatsu, M.; Katayama, T.; Kishimoto, D.; Kurokawa, Y.; Shibata, H.; Ueno, T.; Fujita, T. Quantitative Analyses of the Structure−Hydrophobicity Relationship for *N*-acetyl Di- and Tripeptide Amides. *J. Pharm. Sci.* **1994**, *83*, 1026−1033.
(52) Akamatsu, M.; Fujita, T. Quantitative Analyses of Hydrophobicity of Di- to Pentapeptides Having Un-Ionizable Side Chains with Substituent and Structural Parameters. *J. Pharm. Sci.* **1992**, *81*, 164−174.

CI050450G